# Supporting Information

## *for*

# Coherent phonon dynamics in spatially separated graphene mechanical resonators

Zhuo-Zhi Zhang[1,2†], Xiang-Xiang Song[1,2†*], Gang Luo[1,2†], Zi-Jia Su[1,2], Kai-Long Wang[1,2], Gang Cao[1,2], Hai-Ou Li[1,2], Ming Xiao[1,2], Guang-Can Guo[1,2], Lin Tian[3*], Guang-Wei Deng[1,2*], and Guo-Ping Guo[1,2,4*]

1. Chinese Academy of Sciences Key Laboratory of Quantum Information, University of Science and Technology of China, 230026 Hefei, Anhui, China
2. Chinese Academy of Sciences Center for Excellence in Quantum Information and Quantum Physics, University of Science and Technology of China, 230026 Hefei, Anhui, China
3. School of Nature Sciences, University of California, Merced, CA 95343, USA
4. Quantum Chip Lab, Origin Quantum Computing Company Limited, 230088 Hefei, Anhui, China

† Z.-Z. Zhang, X.-X. Song, and G. Luo contributed equally to this work.

* Correspondence and requests for materials should be addressed to X.-X. Song (songxx90@ustc.edu.cn), L. T. (ltian@ucmerced.edu), G.-W. Deng (gwdeng@ustc.edu.cn), or G.-P. G. (gpguo@ustc.edu.cn).



www.pnas.org/cgi/doi/10.1073/pnas.1916978117

## S1. Gate voltage dependence of resonant frequencies of $R_1$, $R_2$ and $R_3$

The spectra of all three resonators are shown in Fig. S1. Each diagram shows a parabolic-like curve, indicating low built-in stress in our sample[S1]. The avoided level crossings in Fig. S1 represent coupling between the corresponding resonator and other eigenmodes.

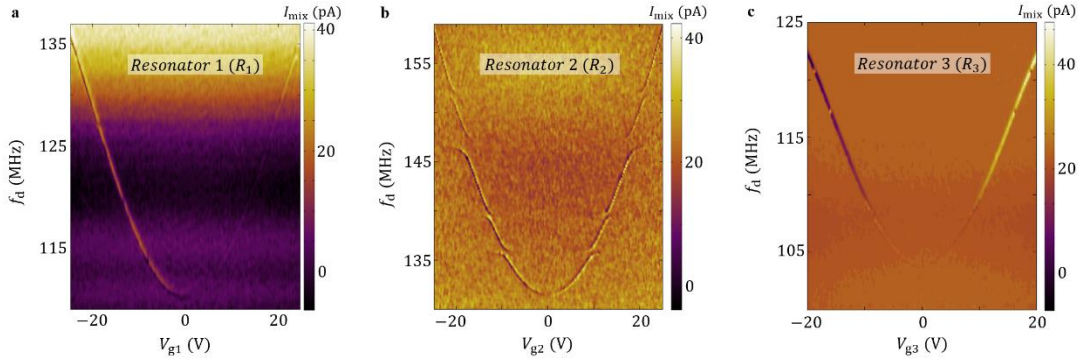


**Fig. S1 Gate voltage dependence of the three resonators' spectra.** The spectra of the three resonators versus their corresponding gate voltages. The data is acquired at driving power of ~ −40 dBm.

## S2. Relaxation rate and quality factor of $R_2$ and $R_3$

Similar to description in the main text for $R_1$, the relaxation rates as well as the quality factors are obtained by fitting the mixing current's dependence on the driving frequency, for both $R_2$ and $R_3$. The data here is fitted with the equation[S2]:

$$I_{mix} \propto \frac{2f_d\left(f_d^2 - f_0^2 - \frac{\gamma f_0}{2\pi}\right)\left(f_d^2 - f_0^2 + \frac{\gamma f_0}{2\pi}\right)}{\left[\left(f_0^2 - f_d^2\right)^2 + \left(\frac{\gamma f_d}{2\pi}\right)^2\right]^2}.$$

Here $f_0$ is the resonant frequency, and $\gamma/2\pi$ the relaxation rate. The extracted relaxation rates and quality factors are $\gamma_2/2\pi \sim 1.16$ kHz, $Q_2 \sim 115{,}000$ for $R_2$, and $\gamma_3/2\pi \sim 0.73$ kHz, $Q_3 \sim 196{,}000$ for $R_3$.

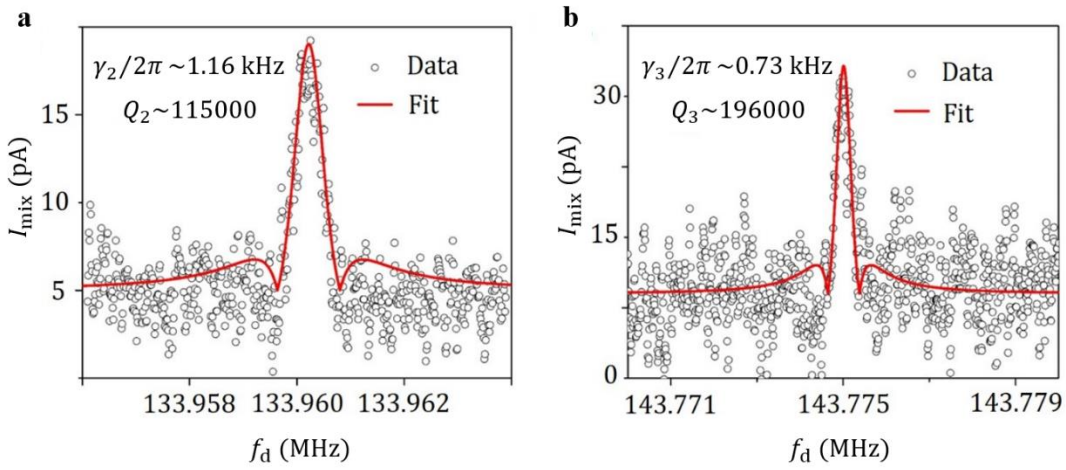


**Fig. S2 Mixing current spectra of $R_2$ and $R_3$ and the fitting of their relaxation rates and quality factors. a.** Mixing current as a function of driving frequency at $V_{g2} = 8$ V. Extracted line width $\gamma_2/2\pi$ of resonator $R_2$, is ~ 1.16 kHz, which gives a quality factor of ~ 115,000. **b.** Mixing current as a function of driving frequency at $V_{g3} = 30$ V. Extracted line width $\gamma_3/2\pi$ of resonator $R_3$, is ~ 0.73 kHz, which gives a quality factor of ~ 196,000. The driving power here is ~ $-60$ dBm.

## S3. Coupling between $R_2$ and $R_3$

An avoided level crossing is observed when tuning the resonant frequency of $R_3$ to approach that of $R_2$, from which we obtain the coupling strength between $R_2$ and $R_3$ to be $\Omega_{23}/2\pi \sim 9$ MHz, as shown in Fig. S3.

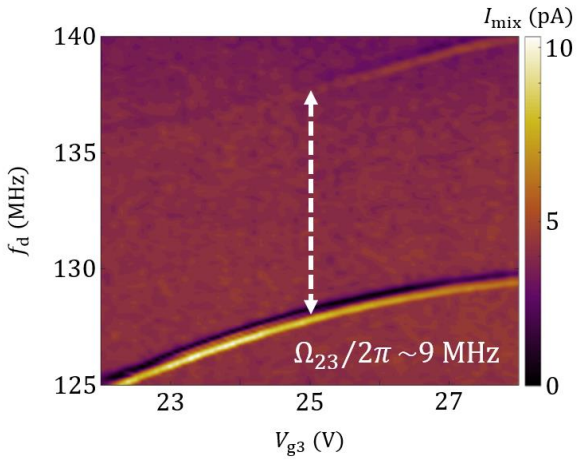


**Fig. S3 Mixing current spectrum of resonators $R_2$ and $R_3$.** Coupling strength $\Omega_{23}/2\pi$ as large as 9 MHz is observed. Here $V_{\mathrm{g1}}$= 0 V and $V_{\mathrm{g2}}$= 8 V. The driving power here is ~ −40 dBm.

## S4. Maximum observed effective coupling strength between resonators $R_1$ and $R_3$

Figs. S4 and S5 show the spectra of the three resonators. We observe a maximum effective coupling strength of $\Omega_{13}/2\pi \sim$ 3.3 MHz, as shown in Figs. S4**a** and S5**a**.

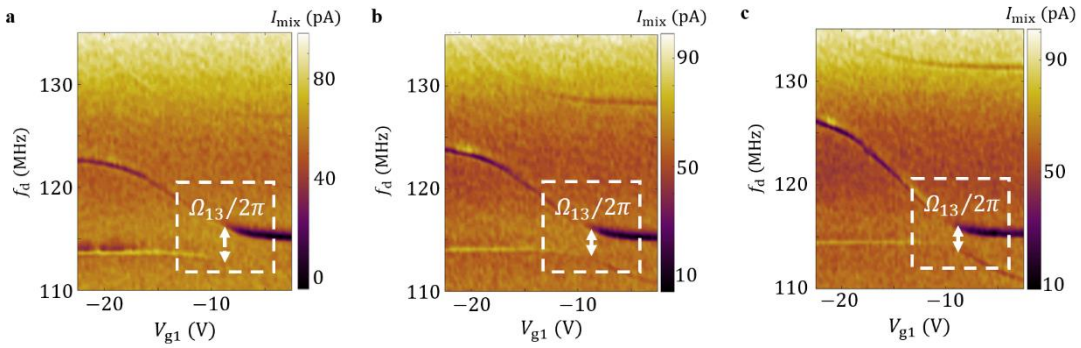


**Fig. S4 Spectra of the three resonators.** Spectra of the three resonators at $V_{g3}$= 15 V, with $V_{g2}$ = 2 V, 6 V, and 10 V for **a-c**, respectively. The zoom-in regime of the white dashed boxes are shown in Fig. S5. The driving power here is ~ −40 dBm.

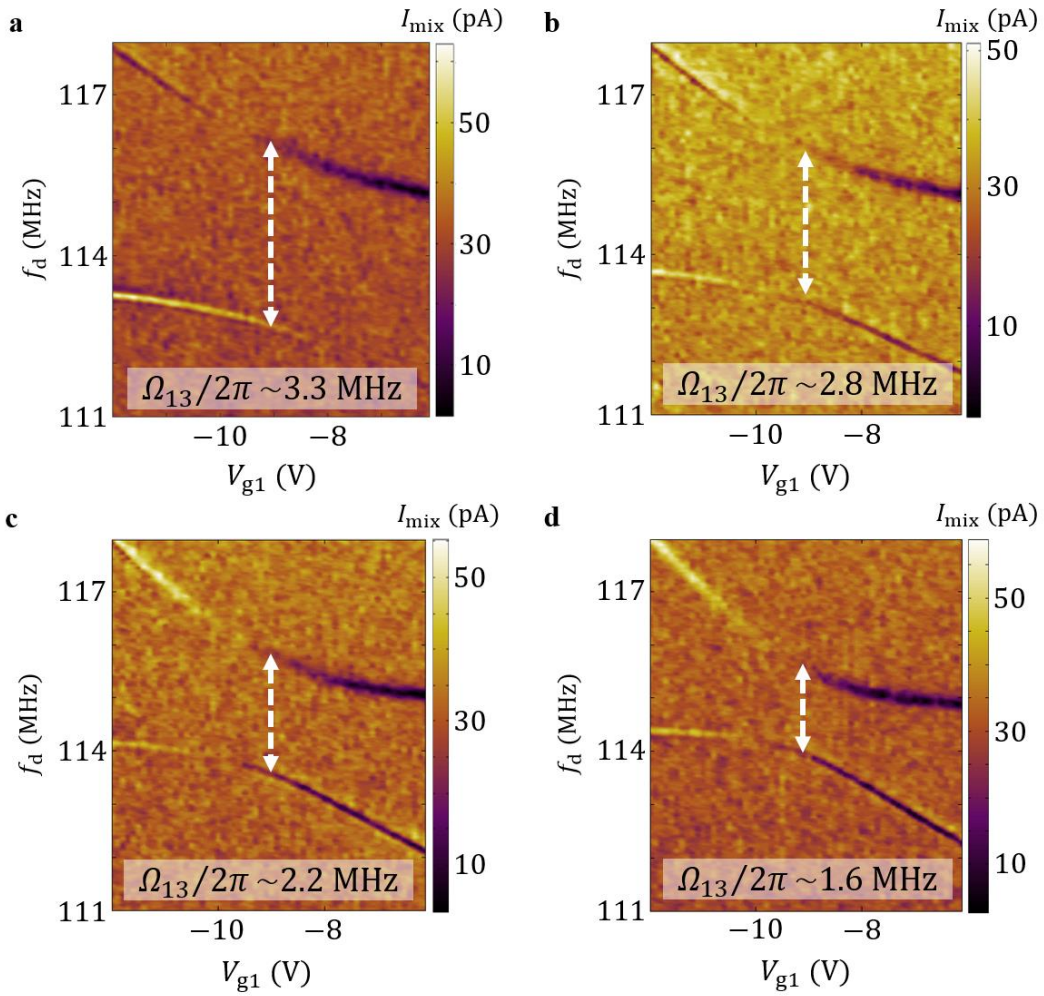


**Fig. S5 Effective coupling between $R_1$ and $R_3$.** Spectra of $R_1$ and $R_3$ at $V_{g3}$= 15 V, with $V_{g2}$ = 2 V, 6 V, 10 V, and 14 V for **a-d**, respectively. **a-c** corresponds to the dashed white box regime in Fig. S4 **a-c**, respectively. **d** corresponds to the similar regime in Fig. 1**e**. Maximum coupling strength as large as 3.3 MHz is observed in **a**. The driving power here is ~ −45 dBm.

**S5. Estimation of phonon number.**

For undriven state, the phonon number can be estimated according to the measurement environment, i.e., the temperature of the dilution refrigerator with $\bar{n}_{th} = 1/(e^{\hbar\omega/k_BT} - 1) \sim 1.61$. Here, $k_B$ is Boltzmann constant, $T$ is around 10 mK, $\omega$ is ~100 $\times 2\pi$ MHz.

For the microwave driven system, taking $R_1$ as an example, from resonant frequency's dependence on gate voltage, we can extract the effective mass[S3] of the graphene to be $m_{eff} \cong 1.43 \times 10^{-17}$ kg (which corresponds to 7.52 layers), see Fig. S6a. Meanwhile, we can obtain equilibrium position displacement $z_e$ to be ~12 nm under gate voltage $V_{g1}$ ~ 15 V (Fig. S6b). Based on the resonant frequency and effective mass, spring constant of a single device is extracted to be $k = m_{eff}\omega^2 \cong 5.64$ N/m, where $\omega$ ~100 $\times 2\pi$ MHz. Using a commercial finite-element analysis simulation software (COMSOL), we calculate gate capacitance $C_g$ as a function of equilibrium position displacement $z_e$ for the device architecture used in our experiment (2 μm in length and 2.2 μm in width), as shown in Fig. S6c and Fig. S6d. The deviation of gate capacitance $C_g'$ remains almost unchanged (6.56 $\times 10^{-10}$ F/m) within the range of $z_e$= 5 to 20 nm. We can also estimate the driving force[S4] according to geometry factor and driving power to be $F_{drive} = C_g' V_g^{DC} \delta V_g \cong 1.97 \times 10^{-11}$ N, here $V_g^{DC}$ and $\delta V_g$ is roughly estimated to be 15 V and 2 mV. Here, $\delta V_g$ is microwave amplitude measured before the sample holder, while considering the absorption efficiency, the power actually sensed by the suspended graphene ribbon should be much lower than this value. With $F_{drive} = kx/Q$ and driven state $Q$~ 300, displacement of

the resonator $x$ can be estimated to be $\cong$ $1.05 \times 10^{-9}$ m. Using $\frac{1}{2}kx^2 \sim n\hbar\omega$, we can estimate the phonon number under microwave driven to have the order of $4.69 \times 10^7$.

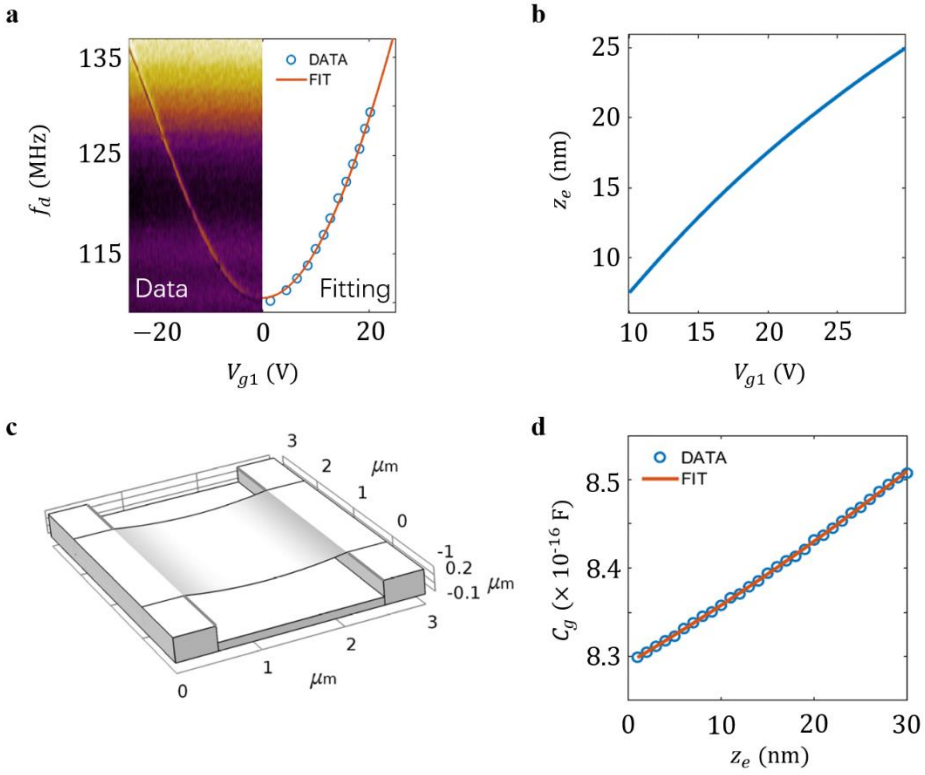


**Fig. S6 Extraction of effective mass and gate capacitance of $R_1$. a**. Fitting of effective mass from spectra of $R_1$, with data from Fig. S1**a**. **b**. Calculated equilibrium position displacement, $z_e$, versus gate voltage $V_{g1}$. **c**. Schematics of device architecture used in our experiments for COMSOL simulations. **d**. Calculated gate capacitance $C_g$ versus equilibrium position displacement, $z_e$. $C_g'$ is estimated to be $6.56 \times 10^{-10}$ F/m.

**S6. Fitting results of Rabi oscillations with different burst power in Fig. 2**

We fitted the Rabi oscillations in Fig. 2 with a damped cosinusoidal function and listed the extracted $T_{\mathrm{Rabi}}$ with the corresponding burst microwave amplitude in Table S1. $T_{\mathrm{Rabi}}$ increases with decreasing $V_{\mathrm{pp}}$. A possible explanation is that decreasing microwave perturbation helps to maintain a longer decoherence time.

| Burst Microwave Amplitude $V_{\mathrm{pp}}$ (V) | Extracted $T_{\mathrm{Rabi}}$ (μs) |
|---|---|
| 0.60 | $11.67 \pm 1.08$ |
| 0.54 | $11.90 \pm 1.15$ |
| 0.48 | $14.75 \pm 1.22$ |
| 0.42 | $12.89 \pm 1.26$ |
| 0.36 | $14.34 \pm 1.01$ |
| 0.30 | $24.34 \pm 3.27$ |
| 0.24 | $25.76 \pm 3.25$ |

**Table S1 Extracted $T_{\mathrm{Rabi}}$ for different burst microwave amplitudes in Fig. 2.**

## S7. Eigenmodes $A$ and $B$ and their dynamics

Following our approach in the previous work and under the rotating-wave approximation[S5], the effective coupling between resonators $R_1$ and $R_3$ can be written as

$$H_I = \frac{\Omega_{13}}{2}(\alpha_1^*\alpha_3 + \alpha_3^*\alpha_1),$$

where $\Omega_{13}$ is the effective coupling strength, the coherent amplitude $\alpha_i = (\sqrt{\omega_{mi}/2}\, x_i + i\sqrt{1/2\omega_{mi}}\, p_i)$ is related to the mechanical displacement $x_i$ and momentum $p_i$, and $\alpha_i^*$ is the complex conjugate of $\alpha_i$. Under this coupling, the eigenmodes of the coupled system of $R_1$ and $R_3$ become $A$ and $B$, with an energy shift $\delta_A = -\Omega_{13}/2$ for mode $A$ and energy shift $\delta_B = \Omega_{13}/2$ for mode $B$. We denote the coherent amplitudes for these eigenmodes as $\alpha_A$ and $\alpha_B$, respectively, with $\alpha_A = (\alpha_1 + \alpha_3)/\sqrt{2}$ and $\alpha_B = (\alpha_1 - \alpha_3)/\sqrt{2}$. The Hamiltonian of this system in the eigenmode basis can be written as

$$H_I^{(en)} = \frac{\Omega_{13}}{2}(\alpha_B^*\alpha_B - \alpha_A^*\alpha_A).$$

During the coherent evolutions studied in our experiment, the initial excitation is set in mode $A$ with a finite amplitude $\alpha_A(0) = \alpha_0$ and with $\alpha_B(0) = 0$. In a Rabi rotation, the external drive mixes the excitations in the eigenmodes. In the eigenmode basis, the driving Hamiltonian can be written as

$$H_{\mathrm{Rabi}}^{(en)} = \frac{\Omega_{\mathrm{Rabi}}}{2}(\alpha_A^*\alpha_B + \alpha_B^*\alpha_A)$$

with $\Omega_{\mathrm{Rabi}}$ being the Rabi frequency. Using a Lagrangian approach, the equations of motion that govern this system are

$$\frac{d\alpha_A}{dt} = -i\frac{\Omega_{\mathrm{Rabi}}}{2}\alpha_B,$$

$$\frac{d\alpha_B}{dt} = -i\frac{\Omega_{\text{Rabi}}}{2}\alpha_A.$$

The dynamics of the system can be understood by solving these equations. Similarly, during the Ramsey interference experiment, the dynamics can be analysed.

**S8. Theoretical analysis of damping times**

The open-system dynamics of the coupled (classical) resonators is different from that of the quantum two-level system. In a standard quantum two-level system, the decoherence rates determine the coherent dynamics are $1/T_1$ and $1/T_2$, respectively, with $1/T_2 = 1/2T_1 + 1/T_\varphi$. Here $1/T_1$ is the relaxation rate between two normal modes $\alpha_{A,B}$ and $T_\varphi$ is the pure dephasing rate between these two modes. As is well known, a Rabi oscillation decays with the rate $(1/T_1 + 1/T_2)/2$, and a Ramsey oscillation decays with the rate $1/T_2$.

The damping rates of our system is very different from that of the standard Bloch equation. We have two classical modes $R_1$ and $R_3$ coupled to each other via an effective coupling $\Omega_{13}$. Assume that the uncoupled mode $R_1(R_3)$ has a relaxation rate $\gamma_1(\gamma_3)$. We also let $\bar{\gamma} = (\gamma_1 + \gamma_3)/2$ be the average of the two rates and $\gamma_d = \gamma_1 - \gamma_3$ be the difference. Without coupling, such relaxation causes the uncoupled modes to relax to their corresponding thermal equilibrium at finite temperature. This is in sharp contrast to the relaxation characterized by $1/T_1$ in a quantum two-level system. This relaxation will bring the system out of the subspace that corresponds to the coherent oscillations between modes $R_1$ and $R_3$.

Let the system be prepared in the normal mode $\alpha_A$ at time $t = 0$, i.e., $\alpha_A(0) = \alpha_0$ and $\alpha_B(0) = 0$, with the excitation amplitude $\alpha_0$. Under this condition, $\alpha_1(0) = \alpha_3(0) = \alpha_0/\sqrt{2}$. Without any pulse applied to this system, the time evolution of the amplitude can be written as $\alpha_A(t) = [e^{-\gamma_1 t/2}\alpha_1(0) + e^{-\gamma_3 t/2}\alpha_3(0)]/\sqrt{2}$. Hence, $\alpha_A(t) = \alpha_0(e^{-\gamma_1 t/2} + e^{-\gamma_3 t/2})/2$. When $\bar{\gamma} \gg \gamma_d$, this can be simplified as $\alpha_A(t) =$

$e^{-\frac{\bar{\gamma}t}{2}}\alpha_0$. It can be shown this will add a damping term $\bar{\gamma}$ in the Bloch equation, as discussed in Ref. S6.

Because the intrinsic relaxation and the dephasing rates between the two modes are much less than $\gamma_i$ ($i$ =1,3), their effects can be neglected. This relaxation times in the coherent oscillations are hence $T_{\mathrm{Rabi}} = T_{\mathrm{Ramsey}} = 2/\bar{\gamma}$. In the spectrum experiment, we obtained $\gamma_i/2\pi \approx 300$ kHz. The results indicates that the relaxation times are at the order of $1$ μs, which is comparable with $T_{\mathrm{Rabi}}$ and $T_{\mathrm{Ramsey}}$ we extracted in the experiments.

## References for Supporting Information:


S1. Chen, C. Y. *et al.* Performance of monolayer graphene nanomechanical resonators with electrical readout. *Nat. Nanotechnol.* **4**, 861-867 (2009).

S2. Gouttenoire, V. *et al.* Digital and FM demodulation of a doubly clamped single-walled carbon-nanotube oscillator: towards a nanotube cellphone. *Small* **6,** 1060-1065 (2010).

S3. Eichler, A. *et al.* Nonlinear damping in mechanical resonators made from carbon nanotubes and graphene. *Nat. Nanotechnol.* **6,** 339-342 (2010).

S4. Sazonova, V. *et al.* A tunable carbon nanotube electromechanical oscillator. *Nature* **431,** 284-287 (2004).

S5. Luo, G. *et al.* Strong indirect coupling between graphene-based mechanical resonators via a phonon cavity. *Nat. Commun.* **9**, 383 (2018).

S6. Faust, T. *et al.* Coherent control of a classical nanomechanical two-level system. *Nat. Phys.* **9,** 485–488 (2013).